2024 IEEE/SICE International Symposium on System Integration (SII)
January 8-11, 2024. Ha Long, Vietnam

A Real-Time Multi-Camera Auto-Adjustment Framework for Infrastructure Inspections

Chuong Phuoc Le[1], Charles Ellison[2], Steven Bunkley[2], Hung La[1], Anton Netchaev[2]

Abstract— **In this paper, we proposed a novel multi-camera auto-adjustment framework for infrastructure inspections, specifically 3D point cloud mapping via lidar-camera fusion. Our method uses a single controller for consensus target brightness and adaptive lighting. In addition, a vignette correction filter was created to apply to images outputted from cameras to avoid dark strips on the point cloud data. This approach is designed to be a versatile, real-time friendly, and platform agnostic software stack.**

I. Introduction

Regular, timely, and thorough inspections are essential for maintaining structures and ensuring their safe use. However, high-quality inspections require a significant time commitment from highly skilled inspectors. Robotics has the potential to both reduce labor and increase the overall quality of inspections by taking over the redundant (i.e., boring), dirty and hazardous parts of the inspection process, allowing inspectors to use their time more efficiently. As a result, the development of novel robotic platforms has received considerable attention in recent years within the field of Structural Health Monitoring as a means for improving inspection processes.

The United States Army Corps of Engineers (USACE) recognizes the potential for improving inspection outcomes through robotics and is developing tools and methods for robotic inspection. One area of focus is on thorough, multi-sensor infrastructure mapping to generate a detailed record of the structure during each inspection that can be compared to past and future inspections for change detection.

As an effort to ensure safety and accuracy in the inspection process, USACE Engineer Research and Development Center (ERDC) has developed an amphibious unmanned ground vehicle (UGV), called the DamBot™ [1], equipped with multiple sensors, which can be remotely controlled to perform first-look inspection. The platform is capable of real time Simultaneous Localization and Mapping (SLAM) using RTABMAP [2].

Fig. 1. Manual inspection has an inspector in the dark with a camera and a flashlight. This method is work-intensive, dangerous, and time-consuming. In contrast, we can have a multi-cam UGV with LED driving through collecting data faster with better accuracy.

The DamBot™ is designed to inspect large underground conduits (10+ m diameter), as shown in Figure 1. Having a robotic inspection platform eliminates several risk factors including bad air, poor evacuation paths, and the potential of tunnel collapse or sudden release of water.

A. Background

To quantitatively evaluate the structural health of infrastructure, it is crucial to capture clean and consistent images of all deterioration, including cracks, corrosion, concrete spalling, water leaks, etc. It is equally important to accurately document the location of each image so the deterioration can be appropriately tracked.

While our overall inspection results with the DamBot™ have been good, there are still problems related to image quality. In this paper, we focus on improving the image pre-processing and/or post-processing of machine vision camera data to ensure good image quality and improve 3D Mapping and Localization during inspection.

To that end, well-exposed and low-noise images are crucial to the vision systems on mobile/robotic inspection platforms. While cameras with built-in Auto-Brightness algorithms are common, they are not always versatile enough to meet the needs of a specific application, making a custom off-device algorithm advantageous. Further, with multi-camera setups, it is crucial to be consistent between cameras, which cannot be accomplished with the onboard algorithms on typical cameras. Each camera has a different perspective, i.e., it

The use of trade, product, or firm names in this report is for descriptive purposes only and does not imply endorsement by the U.S. Government. The tests described and the resulting data presented herein were obtained from research conducted under the USACE Civil Works Flood and Coastal Systems R&D funding. The views, opinions, findings, and conclusions reflected in this publication are solely those of the authors and do not represent the official policy or position of the ERDC, USACE, or the Department of Defense.

This work was also partially funded by the U.S. National Science Foundation (NSF) under grants NSF-CAREER: 1846513 and NSF-PFI-TT: 1919127.

[1]Chuong Le and Hung La are with the Advanced Robotics and Automation (ARA) Lab, Department of Computer Science and Engineering, University of Nevada, Reno, NV 89557, USA.

[2] Steven Bunkley, Charles Ellison, and Anton Netchaev are with the USACE Engineer Research and Development Center (ERDC), Information Technology Lab, Vicksburg, MS 39180, USA.

2024 IEEE/SICE International Symposium on System Integration (SII) | 979-8-3503-1207-2/24/$31.00 ©2024 IEEE | DOI: 10.1109/SII58957.2024.10417321

may see different objects and experience different lighting conditions, and therefore, will make unique adjustments to the image that lead to anomalies when the data is combined.

Therefore, the authors of this report developed custom auto-brightness tools and methods to address the following three issues: (1) good multi-camera fusion requires consistency between devices, consistency is difficult when each camera adjusts hyperparameters like exposure time, gain, and color saturation using its own independent Auto-Exposure (AE), Auto-Gain (AG), and Auto-White-Balance (AWB) algorithms. The result is image anomalies like those in Figure 2. (2) While wide-angle lenses are advantageous in terms of the field of view, they often result in less light toward the sensor's edges, i.e., vignetting. Figure 6 shows an extreme case of vignetting affecting a map. Auto-exposure algorithms and/or gamma correction does not solve this problem. (3) For a mobile robotic platform that frequently works in a dark environment, ambient lighting is insufficient. Active lighting is required, ideally with dynamic control that works in tandem with other auto-brightness approaches. Static light like [3], [4] results in non-colorize or black & light 3D map.

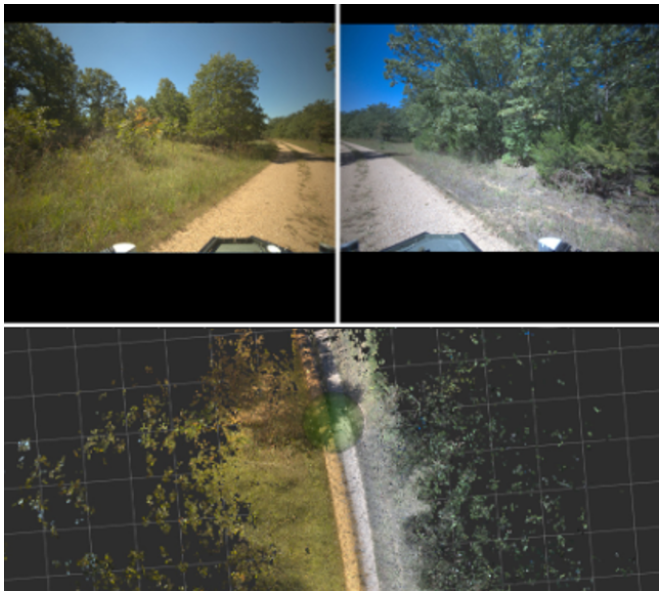

Fig. 2. The images on top are two cameras pointing different directions in the same environment with their independent AE algorithm which provides different lighting. As a result, the point-cloud colorization (bottom image) is split down the middle even though it should be the same. [5]

Since structural inspection is a continuous process, we want to create a robust framework, not just for dams. In this paper, we propose a novel multi-camera auto-adjust framework able to smoothly transition all cameras to reach a consensus brightness by optimizing the exposure time, gain, actively adjusting light level, and applying a vignette correction filter in real time. This framework is designed to be a versatile and platform-agnostic software stack.

II. Outline

This paper is presented in the following order: After the related work in section III, we will be discussing the multi-camera image pipeline used on the Dambot^{TM} in section IV. Then, we will discuss a targeted experimental setup, present the result of our experiment, and evaluate our work in section V. Finally, we will discuss our results' conclusion and future usage in section VI.

III. Related Work

Robotic platforms like Dambot^{TM} present many benefits, mainly because they increase inspection workers' safety and the inspections' repeatability by increasing documentation and avoiding human errors. Prime examples include [6]–[13]. [7], [8] are steel bridge inspection robots utilizing adhesion force generated by permanent magnets to traverse regions of the bridges inaccessible to human inspectors. [12] by Aurora et al. proposed a heterogeneous robotic system using an unmanned ground vehicle with manipulation capability and aerial robots for explorations and 3D mapping in highly unstructured environments. [13] by Gibb et al. uses a UGV equipped with multiple non-destructive evaluations (NDE) sensors and implements a sensor fusion method to perform an in-depth inspection of civil infrastructure like parking garages, bridges, and pavements.

There have been many attempts at auto-exposure methods. Generally, auto-exposure methods adjust the camera exposure time to reach a targeted brightness. Basic approaches consist of measuring the average or median intensity of every pixel of an image, then using some variation of control schemes like the proportional–integral–derivative controller (PID) [14] to achieve a target value. Another approach uses the image intensity histogram metric [15], [16], which is fast but is not robust against complex scenarios. [17] uses an auto-adjusting technique based on image entropy metric for adaptive to different lighting conditions. The drawback of the entropy and histogram approach is that they do not work well in unknown environments since they rely on prior information. Approaches that do not need reference are [18]–[20] based on image gradient techniques to maximize image information via mapping function. However, a significant problem with them is their tendency to over-expose images by favoring high exposure time. To avoid this problem, [21] introduced an image quality metric based on gradient, entropy, and noise and maximized it with the Nelder-Mead (NM) [22] method to obtain well-exposed images by controlling the exposure time and gain parameters. While this method wields good images when it finally converges, the parameter convereargence update is unstable with high, non-smooth oscillation and slow for high-resolution images. Moreover, it works only when cameras are static since the NM method requires two or more (simplex) matching images at different exposure times and gains. In addition, the 3D colorized mapping would be affected due to the constant change in exposure and time to get simplex data.

Most methods control exposure time or gain respectively, but these approaches come at a cost: long exposure time leads to motion blur, while high gain creates image noise. Our approach controls another variable, light level through active lighting. The reason is that we want to minimize the noise

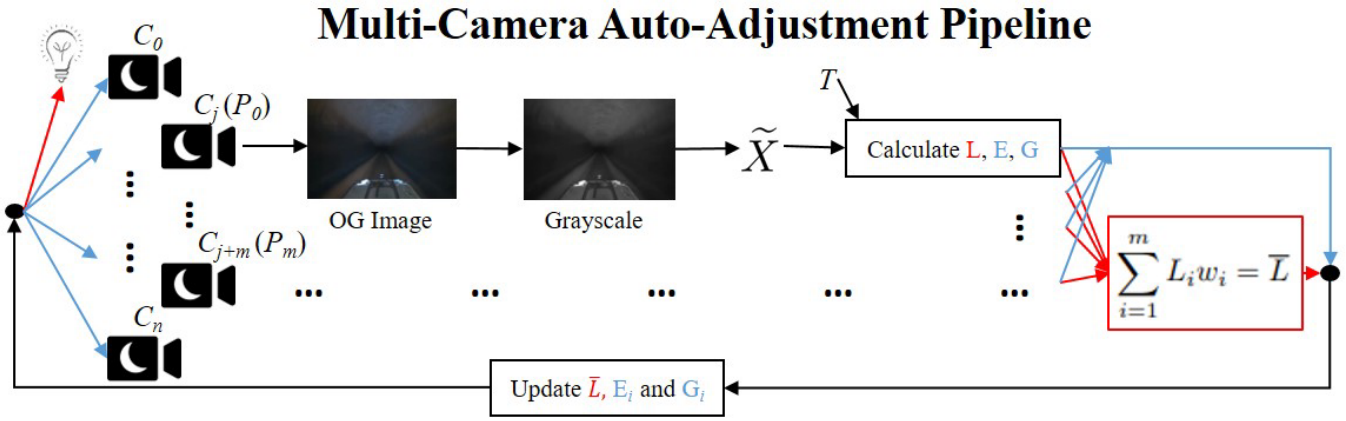

Fig. 3. The flowchart of our multi-cam auto adjustment pipeline.

by minimizing the gain. However, decreasing the gain makes the image received darker, which is compensated by the light level. In addition, our parameter convergence is smooth with low oscillation.

Moreover, while extensive work has been done on single-camera setups, multi-camera auto-adjusting has yet to be given the same attention. For most mobile platforms, including ours, multi-camera setups in different directions are essential for visual odometry, mapping, etc. Acquiring the same brightness images can be difficult, especially in challenging light condition, since each camera has its own independent auto-adjustment algorithm. Current approaches [23], [24] usually require post-processing, which does not work for localization and real-time mapping. In comparison, our multi-camera setup allows an unlimited number of cameras to obtain similar brightness and coherently exposed images.

IV. Method

The DamBot™ project uses GigE protocol cameras capable of sending images and associated meta-data over ethernet to a master processing computer. The cameras can also respond to real-time requests from the computer to change image settings. The cameras are feature-rich and include onboard algorithms to adjust the exposure time, gain, and light level to achieve a target brightness. The image sensors are a Bayer filter mosaic.

In our pipeline, the raw output Bayer images are transferred to the computer in a Bayer RGGB format, leaving the process of up-sampling into a full RGB image for later in the pipeline. This approach provides two immediate benefits: 1) only one-third as much data is transferred over the network 2) vignetting correction can be performed before up-sampling to minimize data processing within the vignette filter.

A control algorithm on the computer is simultaneously monitoring all images for brightness and sending coordinated control signals to the lights and the cameras to regulate lighting, exposure time, and hardware gain. A flowchart of the method is shown in Figure 3.

A. Definition

A simple yet efficient approach for auto-adjusting the images was chosen where all cameras maintain the same setting. However, a subset of the cameras can be used for brightness evaluation. Cameras are defined as

$$\begin{aligned} C &= [C_0, .., C_n], \\ P &= [P_0, .., P_m] \end{aligned} \tag{1}$$

where C is a set of all cameras used with n being the number of cameras used. P is a set of master cameras, with m being the number of master cameras. Since $P \subseteq C$, $m \leq n$. Master cameras are cameras considered a priority; therefore, the only ones considered for light level, L calculations.

The image received from each camera is defined as:

$$\begin{aligned} X &= [x_0, ...x_n], X \in \mathbb{R}^{HxW} \\ \widetilde{X} &= \begin{cases} median(X) & \text{if } M = \text{"median"} \\ mean(X) & \text{otherwise} \end{cases} \end{aligned} \tag{2}$$

where X is image at height and width of H and W. x_i is intensity of pixel i, and $x_i \in [0, 255]$. $\widetilde{X}$ is the average (median or mean) brightness/intensity of image X depending on whether or not the method, M is "median" or "mean."

B. Vignette Correction Filter

Vignette is caused by an attenuation of intensity from the center of the image, creating dark edges around images. The source of our problem is classified as a natural vignette, the falloff due to geometric optics, where different regions of the image plane receive different irradiance. The problem lingers despite attempts to calibrate cameras' settings like aperture and focal length. The dark edges create problems like dark train track-like point cloud data of the robot's path on the map like in Figure 6.

Our vignette correction filter is created by using the lens's brightness percent decay data points from [25]. The curve for aperture of f2.4 and magnification of -0.01 was selected from the referenced report. Then, we fit a fifth-degree polynomial

function to the curve for use in the software, $B(x)$. To fit, we minimize the squared error of a few manually extracted points:

$$E = \sum_{i=0}^{k} |B(x_i) - y_i|^2 \qquad 0 \leq B(x) \leq 1 \tag{3}$$

where k is the amount of data points, and y is the ground truth.

Our correction filter, $F \in \mathbb{R}^{HxW}$ where H and W are the height and width of the filter, which are the same as the image (X) width and height, and

$$\begin{aligned} F_{ij} &= 1 - B(d_{ij}) + 1 \\ d_{ij} &= |p_{ij} - c| \\ |p_{ij} - c| &= \sqrt{[(i - c_r) * p_h]^2 + [(j - c_c) * p_w]^2}, \end{aligned} \tag{4}$$

where F_{ij} is the brightness percent increase at row i and column j and d_{ij} is the is the distance between pixel p_{ij} and the center pixel c, where c_r and c_c is the center row and column respectively. p_h and p_w are the pixel width and height. Since every pixel of the image X_{ij} apart from the center has brightness decrease, the filter applied needs to increase the brightness of X_{ij} element. Hence, all $F_{ij} \geq 1$.

The correction filter F is applied to the image X via cell-wise multiplication.

C. Brightness Controller

To reach certain brightness, we need a controller to change lights and exposure time. To keep it simple, we used a variation of the PID controller with the error representing the difference between the average brightness and target brightness. When multiple master cameras are defined, brightness is simply the mean brightness of all master cameras

$$u(t) = K_p e(t) + \frac{K_i}{\Delta t} \int_{\delta t}^{t} e(t)dt + K_d \frac{de(t)}{dt} \tag{5}$$

that is similar to the regular PID. For the integral part, which accounts for all past values, we instead limited it to δt. For example, if δt = 10, the system will use the last ten values. In addition, we divide the past values by Δt the time between t and δt where $\Delta t = t_{e(t)} - \delta t_{e(t)}$.

D. Weight Distribution

For our multi-consensus controller, we used weight distribution depending on the quality of each image. Hence, we used the quality metric, gradient and entropy from [21]

$$f_i = L_{gradient} + L_{entropy} \tag{6}$$

$$w_i = \frac{f_i}{\sum_{i=0}^{m} f_i} \tag{7}$$

where $\sum_{i=0}^{m} w_i$ = 1. The image with higher quality get weighted more in the computation seen in Algorithm 1 line 15.

Algorithm 1: Multi-Camera Auto-Adjust Control

1 E_p is the previous exposure time
2 L_p is the previous light
3 **Input:** All cameras, C and target brightness, T
4 **for** *each camera* i *in* C **do**
5 (1) Exposure time:
6 - Compute $\widetilde{X}$ from Eq. (2) with T
7 - Compute new Exposure time E_i through auto-exposure using $\widetilde{X}$.
8 (2) Gain:
9 - Compute $\widetilde{X}$ from Eq. (2) with T
10 - Compute new Gain, G_i through auto-gain using $\widetilde{X}$.
11 (3) Light:
12 **if** $j \in P$ **then**
13 - Compute change in light $u_l(t)$ with Eq. (5) and K_l where $e(t) = T - \widetilde{X}$
14 - Compute new light level, $L_j = L_p + u_l(t)$
15 Compute $\overline{L} = \sum_{j=1}^{m} L_j w_j$
16 Send $\overline{L}$ to the LED and E_i and G_i to all camera C

E. Multi-Camera Auto-Adjust Control Algorithm

To achieve brightness consistency for all cameras, we set a consensus target brightness, T, which the weighted brightness value $\widetilde{X}$ needs to reach. We choose median or mean brightness depending on situations, discussed more in section V. Algorithm 1 shows our multi-camera auto-adjust control at every time-step with hyper-parameters k_l, m, T where k_l is a set of $[K_p, K_i, K_d]$ parameters for exposure time and light PID equation 5. m is the number of master cameras. Each camera has an exposure time (1) and gain (2) calculation that utilizes equation 5 as seen in Algorithm 1. For light, a static light is a very inefficient

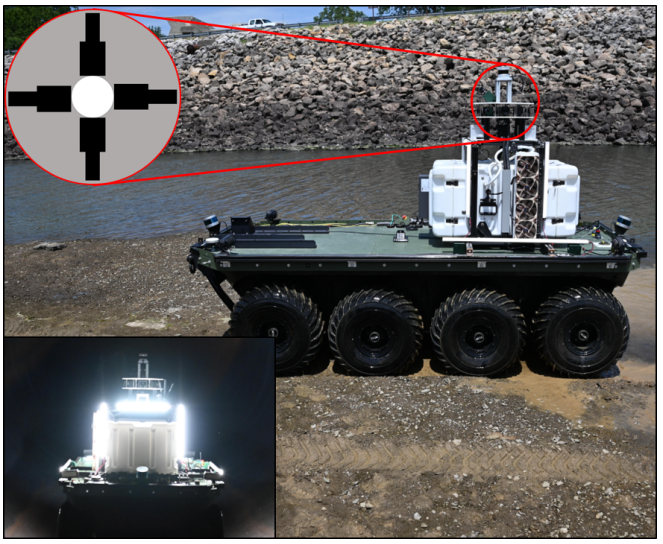

Fig. 4. Our DamBot™ setup: four cameras in each direction, a 360° Ouster LiDAR at the center and LED lights.

power consumption usage. Instead, we have an adaptive light controller that minimizes the light brightness as much as possible while the images' $\widetilde{X}$ still reach T within the exposure and gain limits provided.

V. Experiment

A. Setup

The experimental setup is shown in Figure 4 with four LUCID Atlas 7.1 megapixel cameras with Schneider-Kreuznach lens outputting HxW of 3,208x2,200 resolution images. The main computational power consists of a thirty-two-core AMD Ryzen Threadripper 3970X with 128Gbytes of RAM and an NVIDIA RTX 2080Ti GPU. The multi-camera system is fully calibrated, rectified, and integrated with the LiDAR to create a colorized point cloud.

Power to our lights are controlled by a Talon-SRX motor controller using Pulse-Width-Modulation (PWM) to vary the effective voltage from 0 to 24 volts. The controller has a PWM frequency of 15kHz and outputs is set in terms of a duty cycle, ranges from [0,1] where 0 is 0% and 1 is 100% duty cycle.

Throughout the experiments, we set $p_h = p_w = 0.0045$, $k_l = [3e-3, 1e-4, 1e-4]$, and $T = 64$ all of which were empirically decided. Moreover, we constrained the upper limit of exposure time to 6000 microseconds because it was found to be the threshold for motion blur at typical operating speeds. The maximum gain was limited to 17 dB since it was the maximum value before noise became noticeable in the images. Since speed determines the acceptable exposure time, the team hopes to add dynamic exposure limits based on perceived vehicle speed in upcoming research.

TABLE I

Quality Metric when Converged			
Gradient & Entropy		Entropy	
Mean	**Median**	**Mean**	**Median**
1.55	0.77	0.954	0.853

TABLE II

Duty Cycle in Dark Environment		
Mean	Median	Static
0.36	0.45	1.0
Duty Cycle in Well Lit Environment		
Mean	Median	Static
0	**0**	1.0

B. Result

First, we test both mean and median brightness methods to determine the difference between the two approaches. To do a quantitative test, we used the gradient and entropy metric shown in [21]. We chose gradient and entropy because the gradient metric likes overexposure images; hence, we paired it with entropy. Entropy shows the amount of information contained in the image. As seen in Table I, the usage of mean T outperforms median brightness in terms of these metrics.

Next, we tested the static light against the adaptive light. Our quantitative test compares the usage of power. As seen in Table II, while static light is using full power at all times, the usage of adaptive light varies depending on the environment: it turns uses minimal light while achieving T and will turn completely off when in a well lit environment. In particular, mean T used the least amount of power in a dark environment at 0.36 power or 126 Watts, making it the optimal T. Finally, we test the efficiency of the vignette correction filter. As seen in Figure 5, the correction filter's brightness decay is much less than the raw output, decreasing approximately half as much at around 70% as opposed to 40%. Moreover, while the correction filter failed to negate the irradiance fall-off entirely, it prevented the train-track-like strips from showing up in the point cloud map, as shown in Figure 6. In addition, the processing time of applying of filter was only 30 ms (33.34 Hz) for a large image resolution of 3208x2200, making it very suitable for real-time applications.

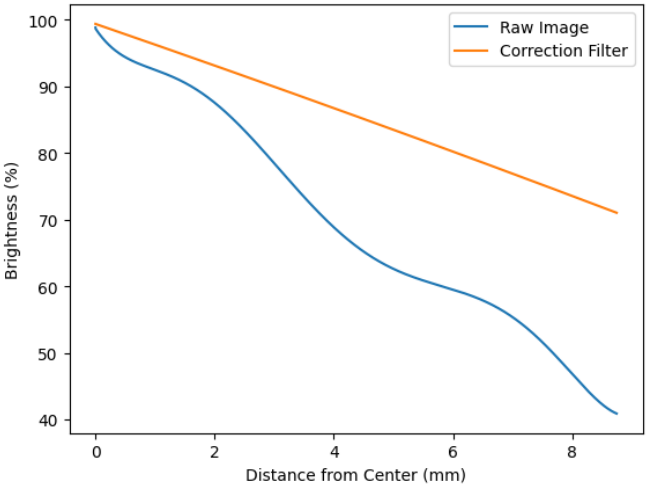

Fig. 5. Image brightness falloff from center of original image and correction filter.

VI. Conclusion and Future Work

In this paper, we present a novel real-time multi-camera auto-adjustment framework for infrastructure inspection, specifically for 3D mapping. Our framework auto-adjust the exposure time, gain, and light level so all camera reached a consensus target brightness while applying a vignette correction filter to the output image. The result was the output images were able to achieve similar brightness sufficient for 3D mapping. In particular, the vignette correction filter was able to remove enough of the vignette to solve the stripping problem on the 3D map, demonstrated in Figure 6. Due to the usage of simple control algorithms and Bayer image format, it was able to run very smoothly in real-time. However, we recognize that average pixel brightness is not a robust enough metric. In addition, our vignette correction filter was not able to fully negate the irradiance fall-off across each image pixels. In the future, we plan to extend our work to a more robust brightness metric while improving our vignette

correction filter to have even brightness percentage across all pixels.

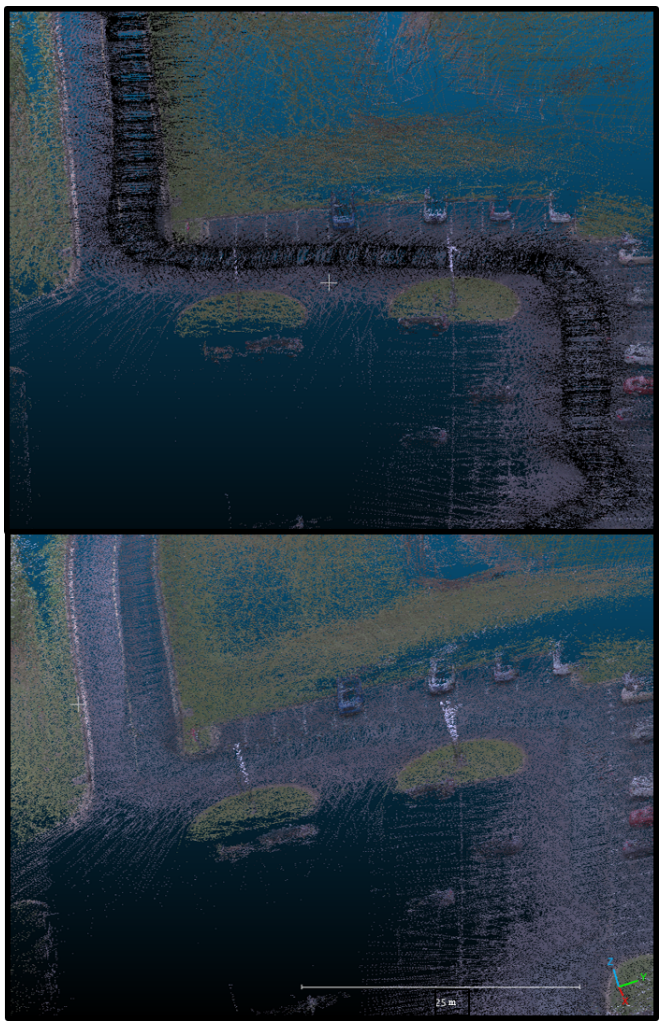

Fig. 6. Point cloud data generated by rtabmap using data from LiDAR and vision cameras. The top image shows data from vision cameras. The bottom image shows data from vision cameras with the vignette correction filter. There's also a 25 meter ruler at the bottom to show the scale.

REFERENCES

[1] J. Klein, S. B. C. Ellison, G. Glaspell, K. Niles, C. Webb, R. B. C. Dickerson, and A. Netchaev, "Dambot™: An unmanned amphibious vehicle for earth dam outlet inspection," *The 14th International Workshop on Structural Health Monitoring (IWSHM)*, 2023.

[2] M. Labbé and F. Michaud, "Rtab-map as an open-source lidar and visual simultaneous localization and mapping library for large-scale and long-term online operation," *Journal of Field Robotics*, vol. 36, no. 2, pp. 416–446, 2019.

[3] F. Mascarich, S. Khattak, C. Papachristos, and K. Alexis, "A multi-modal mapping unit for autonomous exploration and mapping of underground tunnels," in *2018 IEEE Aerospace Conference*, 2018, pp. 1–7.

[4] F. Mascarich, T. Wilson, S. Khattak, T. Dang, C. Papachristos, and K. Alexis, "Autonomous 3d and radiation mapping in tunnel environments using aerial robots–18156."

[5] K. Niles, S. Bunkley, W. J. Wagner, I. Blankenau, A. Netchaev, and A. Soylemezoglu, "Satellite image template matching with covariance estimation for unmanned ground vehicle localization: Active terrain localization imaging system (atlis)," *Ground Vehicle Systems Engineering and Technology Symposium (GVSETS)*, 2022.

[6] P. Arora and C. Papachristos, "Environment reconfiguration planning for autonomous robotic manipulation to overcome mobility constraints," in *2021 IEEE International Conference on Robotics and Automation (ICRA)*, 2021, pp. 2352–2358.

[7] H.-D. Bui, S. Nguyen, U.-H. Billah, C. Le, A. Tavakkoli, and H. M. La, "Control framework for a hybrid-steel bridge inspection robot," in *2020 IEEE/RSJ International Conference on Intelligent Robots and Systems (IROS)*, 2020, pp. 2585–2591.

[8] H. Ahmed, S. T. Nguyen, D. La, C. P. Le, and H. M. La, "Multi-directional bicycle robot for bridge inspection with steel defect detection system," in *2022 IEEE/RSJ International Conference on Intelligent Robots and Systems (IROS)*, 2022, pp. 4617–4624.

[9] A. Q. Pham, C. Motley, S. T. Nguyen, and H. M. La, "A robust and reliable climbing robot for steel structure inspection," in *2022 IEEE/SICE International Symposium on System Integration (SII)*, 2022, pp. 336–343.

[10] C. P. Le, A. Q. Pham, H. M. La, and D. Feil-Seifer, "A multi-robotic system for environmental dirt cleaning," in *2020 IEEE/SICE International Symposium on System Integration (SII)*, 2020, pp. 1294–1299.

[11] S. J. Carlson, B. Moore, T. Karakurt, P. Arora, T. Cooper, and C. Papachristos, "The gannet solar–vtol: An amphibious migratory uav for long–term autonomous missions," in *2023 International Conference on Unmanned Aircraft Systems (ICUAS)*, 2023, pp. 419–424.

[12] P. Arora and C. Papachristos, "Mobile manipulation–based deployment of micro aerial robot scouts through constricted aperture-like ingress points," in *2021 IEEE/RSJ International Conference on Intelligent Robots and Systems (IROS)*, 2021, pp. 6716–6723.

[13] S. Gibb, H. M. La, T. Le, L. Nguyen, R. Schmid, and H. Pham, "Nondestructive evaluation sensor fusion with autonomous robotic system for civil infrastructure inspection," *Journal of Field Robotics*, vol. 35, no. 6, pp. 988–1004, 2018.

[14] K. J. Åström and T. Hägglund, *Advanced PID control*. ISA-The Instrumentation, Systems and Automation Society, 2006.

[15] J. Torres and J. M. Menéndez, "Optimal camera exposure for video surveillance systems by predictive control of shutter speed, aperture, and gain," in *Real-Time Image and Video Processing 2015*, N. Kehtarnavaz and M. F. Carlsohn, Eds., vol. 9400, International Society for Optics and Photonics. SPIE, 2015, p. 94000S.

[16] M. Montalvo, J. M. Guerrero, J. Romeo, M. Guijarro, J. M. de la Cruz, and G. Pajares, "Acquisition of agronomic images with sufficient quality by automatic exposure time control and histogram matching," in *Advanced Concepts for Intelligent Vision Systems*, J. Blanc-Talon, A. Kasinski, W. Philips, D. Popescu, and P. Scheunders, Eds. Cham: Springer International Publishing, 2013, pp. 37–48.

[17] H. Lu, H. Zhang, S. Yang, and Z. Zheng, "Camera parameters auto-adjusting technique for robust robot vision," in *2010 IEEE International Conference on Robotics and Automation*, 2010, pp. 1518–1523.

[18] I. Shim, T.-H. Oh, J.-Y. Lee, J. Choi, D.-G. Choi, and I. S. Kweon, "Gradient-based camera exposure control for outdoor mobile platforms," *IEEE Transactions on Circuits and Systems for Video Technology*, vol. 29, no. 6, pp. 1569–1583, 2019.

[19] I. Mehta, M. Tang, and T. D. Barfoot, "Gradient-based auto-exposure control applied to a self-driving car," in *2020 17th Conference on Computer and Robot Vision (CRV)*. IEEE, 2020, pp. 166–173.

[20] M.-A. Bégin and I. Hunter, "Auto-exposure algorithm for enhanced mobile robot localization in challenging light conditions," *Sensors*, vol. 22, no. 3, 2022.

[21] U. Shin, J. Park, G. Shim, F. Rameau, and I. S. Kweon, "Camera exposure control for robust robot vision with noise-aware image quality assessment," in *2019 IEEE/RSJ International Conference on Intelligent Robots and Systems (IROS)*, 2019, pp. 1165–1172.

[22] J. A. Nelder and R. Mead, "A simplex method for function minimization," *The computer journal*, vol. 7, no. 4, pp. 308–313, 1965.

[23] M. Pollefeys, D. Nistér, J.-M. Frahm, A. Akbarzadeh, P. Mordohai, B. Clipp, C. Engels, D. Gallup, S.-J. Kim, P. Merrell *et al.*, "Detailed real-time urban 3d reconstruction from video," *International Journal of Computer Vision*, vol. 78, pp. 143–167, 2008.

[24] Y. S. Heo, K. M. Lee, and S. U. Lee, "Robust stereo matching using adaptive normalized cross-correlation," *IEEE Transactions on pattern analysis and machine intelligence*, vol. 33, no. 4, pp. 807–822, 2010.

[25] "TOPAZ 2.4/6.5 C," https://schneiderkreuznach.com/application/files/5316/5579/7957/TOPAZ_24_65_C_1088899_datasheet.pdf, [Online; accessed 19-July-2023].